Contract No.:

This manuscript has been authored by Savannah River Nuclear Solutions (SRNS), LLC under Contract No. DE-AC09-08SR22470 with the U.S. Department of Energy (DOE) Office of Environmental Management (EM).

Theoretical and Applied Climatology

Quantifying the Local Influence at a Tall Tower Site in Nocturnal Conditions

--Manuscript Draft--

Manuscript Number:	
Full Title:	Quantifying the Local Influence at a Tall Tower Site in Nocturnal Conditions
Article Type:	Original Paper
Corresponding Author:	David Werth, Ph. D. Atmospheric Technologies Group, Savannah River National Laboratory Aiken, SC UNITED STATES
Corresponding Author Secondary Information:	
Corresponding Author's Institution:	Atmospheric Technologies Group, Savannah River National Laboratory
Corresponding Author's Secondary Institution:	
First Author:	David Werth, Ph. D.
First Author Secondary Information:	
Order of Authors:	David Werth, Ph. D.
	Robert Buckley, Ph. D.
	Gengsheng Zhang, Ph. D.
	Robert Kurzeja, Ph. D.
	Monique Leclerc, Ph. D.
	Henrique Duarte, Ph. D.
	Matthew Parker, M.S.
	Thomas Watson, Ph. D.
Order of Authors Secondary Information:	
Abstract:	The influence of the local terrestrial environment on atmospheric CO2 measurements at a television transmitter tower was estimated through a tracer release experiment, a simulation of the release, and the calculation of eddy diffusivity at the tower site. These are used to characterize the vertical transport of emissions from the surface to the uppermost tower level and how it is affected by atmospheric stability. The tracer release experiment was conducted over two nights in May of 2009 near the Department of Energy's Savannah River Site in South Carolina. Tracer gas was released on two contrasting nights - slightly stable and stable - from several upwind surface locations. Measurements of tracer concentration were made at different levels, and the results suggest the tracer was able to mix vertically within a relatively short (~24km) distance. A simulation of the tracer release is used to calculate the tower footprint on the two nights. The effect of nocturnal stability on the area sampled by the tower can be seen clearly - the footprint indicated a much weaker influence of the local environment on the more stable night, implying a more distant sampling domain. The contribution of local sources to the measurements at the highest level was minimal, however, suggesting that nocturnal concentrations at these levels are contributed mostly by regional sources. The eddy diffusivity was calculated with observed CO2 fluxes as an indicator of observed turbulent transport on the two nights, and compared to the transport inferred from the tracer release and its simulation.
Suggested Reviewers:	Erich Mursch-Radlgruber, Ph.D. Professor, Universiy of Natural Resources and Life Sciences, Vienna erich.mursch-Radlgruber@boku.ac.at
	Jinkyu Hong, Ph. D.

	Professor, Yonsei University jhong@yonsei.kr
	Xuhui Cai, Ph. D. Professor, Peking University xhcai@pku.edu.cn
	Natascha Kljun, Ph. D. Associate Professor, Swansea University n.kljun@swansea.ac.uk

Quantifying the Local Influence at a Tall Tower Site in Nocturnal Conditions

David Werth[1]

Robert Buckley[1]

Gengsheng Zhang[2]

Robert Kurzeja[1]

Monique Leclerc[2]

Henrique Duarte[2]

Matthew Parker[1]

Thomas Watson[3]

[1] Savannah River National Laboratory, Building 773-A, Aiken, SC 29808
[2] Laboratory for Atmospheric and Environmental Physics, University of Georgia, Griffin, GA, USA
[3] Tracer Technology Group, Brookhaven National Laboratory, Upton, NY, USA

Corresponding Author: David Werth, Savannah River National Laboratory, Building 773-A, Aiken, SC 29808, David.Werth@srnl.doe.gov, 803-725-3717, Fax No. 803-725-4233

Abstract

The influence of the local terrestrial environment on atmospheric CO_2 measurements at a television transmitter tower was estimated through a tracer release experiment, a simulation of the release, and the calculation of eddy diffusivity at the tower site. These are used to characterize the vertical transport of emissions from the surface to the uppermost tower level and how it is affected by atmospheric stability.

The tracer release experiment was conducted over two nights in May of 2009 near the Department of Energy's Savannah River Site in South Carolina. Tracer gas was released on two contrasting nights - slightly stable and stable - from several upwind surface locations. Measurements of tracer concentration were made at different levels, and the results suggest the tracer was able to mix vertically within a relatively short (~24km) distance.

A simulation of the tracer release is used to calculate the tower footprint on the two nights. The effect of nocturnal stability on the area sampled by the tower can be seen clearly - the footprint indicated a much weaker influence of the local environment on the more stable night, implying a more distant sampling domain. The contribution of local sources to the measurements at the highest level was minimal, however, suggesting that nocturnal concentrations at these levels are contributed mostly by regional sources. The eddy diffusivity was calculated with observed CO_2 fluxes as an indicator of observed turbulent transport on the two nights, and compared to the transport inferred from the tracer release and its simulation.

1. Introduction

In contrast with the multitude of studies of vertical transport in the convective boundary layer (e.g., Wang et al. 2007; Barkhatov et al. 2012), vertical transport modeling and measurements in the stable boundary layer remain scarce (Sogachev and Leclerc 2011). This lack of robust data can hinder the interpretation of measurements made at a tall tower sampling platform under stable conditions. If measurements at a tower site are to be used to constrain global-scale carbon budgets, they should be representative of continental-scale CO_2 distributions (Desai 2008). The surface area over which emissions are detected at an upper tower level is dictated by the local meteorology, especially the atmospheric stability (Gerbig et al. 2009; Sogachev and Leclerc 2011; Gloor 2001). Stable conditions often prevail during nighttime, making such periods ideal for continental-scale sampling (Gloor et al. 2001). Nocturnal turbulent conditions do occur, however, depending on the local terrain and meteorology, and the sampled area will tend to be local if there is significant vertical mixing of respired CO_2 (Gerbig et al. 2009). In their paper on continental carbon exchange, Gerbig et al. (2009) describe the issues involved in the design and interpretation of a tower network, and write "In a network of tall towers, the most important [question] is to ask: 'what is it that the individual tower observes?'". We need to know more about nocturnal eddy transport and the influence of the nearby environment on a tower.

The area sampled by a tower in any particular condition is often described by its 'footprint'- a function that weights the contribution from each point at the surface to the measured signal (Schuepp et al. 1990; Leclerc and Thurtell 1990; Rannik et al. 2003; Sogachev et al., 2005; Cai et al. 2008; Gerbig et al. 2009; Sogachev and Leclerc 2011; Barcza et al. 2009; Chen et al. 2012; Chen et al. 2013). The calculation of a footprint is often accomplished with a transport model that uses as input either a meteorological reanalysis (Gloor et al. 2001; Gerbig et al. 2009; Hegarty et al. 2013) or a boundary-layer model (Sogachev and Leclerc 2011). As the planetary boundary layer (PBL) becomes more turbulent, the footprint will be confined to an area near the tower as vertical mixing will quickly move CO_2 upwards. Gerbig et al. (2009), for example, used the Stochastic Time-Inverted Lagrangian Transport (STILT) transport model with an analyzed wind field to estimate footprints of the 30m level of the Harvard Forest tower in turbulent daytime conditions (when

mixing leads to small differences between the 30m and 300m levels), and noted the dominant influence within 20km of the tower. In stable conditions, however, the footprint should begin at a surface point well away from the tower and extend for long distances (Sogachev and Leclerc 2011).

In August 2008, the "South Carolina Tower" (SCT), a 457m television transmitter tower near Beech Island, SC, was incorporated into the National Oceanic and Atmospheric Administration's (NOAA) tall tower network (a subset of the Ameriflux network). The SCT site is located within a region characterized by broken forests and agriculture in the immediate vicinity, with suburban, urban, and industrial areas (most notably Augusta, GA) within 20km. As with any tower, the contribution of these carbon sources to the concentrations measured at the tower must be quantified, and our goal is to determine the location of sources contributing to the flux signature measured at the SCT tower.

The objective of this paper is to obtain detailed information about the way eddy activity acts to move a gas emitted from the surface near the SCT upward to higher levels in the absence of convection. To accomplish this, a set of artificial tracers was released into the nocturnal boundary layer (NBL) on two nights from various locations within a 24km distance upwind of the tower (Parker et al., in preparation) and time series of measurements at three tower levels were recorded. The source area around a tower can be characterized by a 'near-field' (within ~50km) and a 'far-field' out to the order of 1000km (Gerbig et al. 2009), and the focus here is on the SCT near-field. Therefore, a high-resolution mesoscale PBL simulation of a 19km x 26km domain (encompassing the area of the experiment) is coupled to a transport model of the tracer release and validated against the tracer signal at the tower. The coupled model is then used to estimate the footprints on the two nights.

Sogachev and Leclerc (2011) applied the Scalar Distribution (SCADIS) boundary layer model with a Lagrangian transport model to estimate footprints in the stable boundary layer, and they found that 'the changing atmospheric stratification determines the footprint which depends not only on the height of a sensor, but also on the time of measurements'. They also note that the calculation of a footprint can be made more robust with the inclusion of actual data for comparison, and this is the goal of the current research.

Turbulent transport on the two nights is also characterized by their vertical eddy diffusivity values, calculated using the observed CO_2 fluxes and concentrations. With the tracer, footprint, and diffusivity information, we hope to understand better the degree to which the SCT is influenced by the local environment.

2. Tracer Field Experiment

Tracer releases are a well-established method to study atmospheric motions (van Dop et al. 1998; Leclerc et al. 2003a, b), but their use to study stable boundary layers is less common. A nocturnal tracer study was conducted at the SCT site in May 2009 (Parker et al. in preparation), with the goal of evaluating the way gas released from the area near the tall tower is mixed upward into the stable or slightly stable boundary layer during lateral advection. The experiment comprised the released tracers and their detection at various heights on the SCT, and the data was then used to validate a simulation of the release. A tracer release was conducted on each of two nights – a slightly-stable night (May 11th/12th, 2009), and a second, more stable night (May 12th/13th, 2009), identified as such by their temperature profiles, the values of the bulk Richardson number (Ri) calculated between the upper two tower levels, and Vaisala CL31 (Helsinki, Finland) lidar ceilometer readings of the boundary layer height. Compared to Night 1, Night 2 has a stronger inversion, higher Ri values, and a shallower mixing layer (Figure 1). This will allow for the study of tracer behavior as a function of stability. Selected tracer data from this field experiment and local meteorological measurements are used in this study (Parker et al., in preparation).

2.1 Experimental Design

A set of release points was established from about 3km to 24km in the quadrant northeast of the tall tower (Fig. 2), which was equipped with sampling tubes at elevations of 34m, 68m and 329m above ground level. A set of five perfluorocarbon (PFC) tracers (Table 1) was selected, and each release point was assigned a single tracer with a standard release rate (Table 2). The tracers were deployed to minimize overlapping of plumes containing the same tracer when both were upwind of the tower (Table 1). In this way, the release point associated with any tracer signal can be identified.

The field experiment took place in May 2009, with the tracer release beginning at midnight EDT (0400 UTC) for all tracers except for PTCH, which began releasing at 2:00am EDT (0600 UTC) from the most distant locations.

The tall tower was equipped with several types of sensors – a tube sampler for the tracer, a (NOAA) tube sampler for CO_2, an open-path infrared gas analyzer for CO_2 and water vapor (Licor Model 7500), and a sonic anemometer (ATI Model S_a, ATI Model S_x) to measure the three-dimensional wind components and, through its measurements of wind speed variability, virtual temperature. The sensors and tube sampler inlets were deployed at three levels: 34m, 68m and 329m. The tube samplers have been discussed in Parker et al. (in preparation), and the reader is referred there for a detailed description.

In addition to the tower data, a sodar with a radio acoustic sounding system (RASS) extension (Scintec AG, model SFAS, Rottenburg, Germany) was installed at 33.455N, 81.7739W, within about the center of the experiment domain (Fig. 2), providing temperature and wind data throughout the vertical extent of the boundary layer. A second sodar (Remtech PA2) was installed at 33.340N, 81.564W (Fig. 2), providing another source of wind data throughout the depth of the boundary layer.

2.2. Experimental Results

2.2.1 Night 1: 11 to 12 May, 2009 – Slightly Stable Case

The tower readings reveal that boundary layer winds came from the northeast quadrant the entire night at all levels (Fig. 3a), in agreement with the Remtech sodar (Fig. 4a). Winds at upper levels gradually slowed as the night progressed (Fig. 4a). Assuming a relatively uniform wind field over the domain, this implies that release points 3, 4, 5, 6, 7, 10, 11 and WA, with their different tracers, were each upwind of SCT at sometime during the night as the wind shifted (Fig. 2), leading to detection of their respective tracers. Tracer PMCH was released from Point 4 (Table 1), and this nearby point produces a signal near the surface at SCT within one hour (Fig. 5a). As the winds shifted from 60° to 45° later in the night (Fig. 3a), PMCH emissions from Point 10 impacted SCT by 5:00am EDT (0900 UTC) (Fig. 5a), also in a short time. Late in the night the PTCH tracer from

point WA (the most distant point) reached the tower about three hours after the tracer release started at 2:00am EDT (0600 UTC) (Fig. 5b).

It might be expected that tracer would be completely confined beneath the boundary layer heights in Fig 1c or that only the more distant tracers would be able to mix up to 329m before reaching the tower. Fig. 5a, however, shows that even tracer from Point 4 was able to mix upwards to 329m within a relatively short distance (8-13 km) (329m data are missing from 2am to 4am). Values at the two levels were nearly identical following the period of stronger mixing between 0400UTC and 0800UTC implied by the smaller Richardson values in Fig. 1b. Tracer PTCH from Point WA was able to mix upward in greater concentrations within its longer transport distance of 22 km (Fig. 5b). The close-in source experiences weaker vertical mixing - the ratio of the maximum values at 329m and 34m is larger for the more distantly-released tracer.

2.2.2 Night 2: 12 to 13 May, 2009 – Stable Night

On Night 2, boundary layer winds started off from the southeast (Figs. 3b, 4b), forcing the tracer away from the tower, but gradually shifted northward (Fig. 3b), allowing for a detectable signal. A weak low-level jet (LLJ) formed at about 4:00am EDT (0800 UTC) (Fig. 4b), and strengthened over the next 4 hours, reaching a maximum at 8:00am EDT (1200 UTC). The PDCB tracer was released from points due east (Pt. 3) and NE (Pt. 6) of the tower, and 'pulses' of tracer passing over the sensor are seen as the upwind direction shifts from one source to the other (Fig. 5c). A signal from Pt. UE arrives later in the night as it traverses the 24km distance from release to tower (Fig. 5d). Both tracers were able to mix significantly in the vertical before reaching the tower (despite the low boundary layer heights present on both nights as seen in Fig. 1c), but on Night 2 the most distant tracer peaks at only about 1/3 its surface concentration, whereas on Night 1 the tracer is able to mix upward in quantities sufficient to cause the ratio of the peaks to be over half (albeit briefly), implying the vertical mixing of the tracer was weaker on the more stable second night.

3. Tracer Simulation

3.1 Models

Calculating the motion of the tracer and inferring the relationship between the vertical transport and the turbulent properties of the atmosphere requires knowing the emission rate of the source, as well as estimates of the advection and turbulent transport terms. While the emission rate in this study is known (Table 2), modeling must be used to estimate the advection and turbulent terms. Similar to the work of Sogachev and Leclerc (2011), a meteorological model was coupled to a dispersion model to explicitly calculate the tracer concentrations at each point which were used to get the full budget and calculate the tower footprint at various times. The mesoscale simulation of winds and turbulence from each night effectively serves as a reanalysis of the tracer release domain. Coupled dispersion simulations often lack observed concentrations against which to validate the model results (Sogachev and Leclerc 2011), but our tracer data can be used to validate our coupled simulation.

3.1.1 RAMS

The Regional Atmospheric Modeling System (RAMS, Pielke et al. 1992) has been used previously to simulate fine-scale motions within the nocturnal boundary layer (e.g., Werth et al. 2011), and is selected to recreate the meteorology from the two nights of the tracer experiment, centered over the domain in Fig. 6a. RAMS solves the nonhydrostatic equations of motion for velocity and potential temperature on a staggered C grid (Mesinger and Arakawa 1976) on a polar stereographic grid. The model also employs a terrain-following sigma coordinate system in the vertical. For our purposes, an innermost domain of 200m grid spacing was designed covering the area of the experiment (25.8km x 19.4km). This grid is nested within coarser grids as described below. The Harrington radiation scheme (Harrington 1997) is applied for both shortwave and longwave radiative transfer. For convection, the Kuo scheme (Kuo 1974) is applied for the coarser grids, while the innermost, 200m grid uses an explicit cloud prognostic scheme (Cotton et al. 1986; Meyers et al. 1992). A Newtonian 'nudging' of all grids is applied, by which the outer boundary of each grid is adjusted towards the values of its parent grid (Clark and Hall 1991), with the influence

of the parent gradually diminishing towards the center of the domain. Two-way nesting is applied, allowing each inner grid to in turn influence its respective parent.

The RAMS surface must be assigned values of topography and land cover, as well as an initial profile of soil heat content. For the innermost grid, the topography comes from a high resolution (3") dataset (Fig. 6b), while the coarser grids use a 30" digital elevation model dataset. Surface fluxes are calculated according to the LEAF-3 land surface scheme (Walko et al. 2000). Each grid square is partitioned into 21 land surface types, based on 1km U.S. Geological Survey data, and the surface fluxes are calculated according to the surface variables (leaf area index, albedo, etc.) associated with each type. Soil heat content is assigned an initial uniform value that leads to the best simulation of the observed nocturnal boundary layers.

The model is run twice – once for the period May 11th, 2009 at 2:00pm EDT (1800 UTC) to May 12th, 2009 at 8:00am EDT (1200 UTC) (Night 1), and again for the period May 12th, 2009 at 2:00pm EDT (1800 UTC) to May 13th, 2009 at 8:00am EDT (1200 UTC) (Night 2). Besides the dates, several important differences exist between the two simulations. On the first night, the model is run with nested grids of 3200m, 800m, and 200m, with the 13.5km resolution Rapid Update Cycle (RUC) product used as the boundary conditions (Benjamin et al. 2004). For Night 2, however, the RUC boundary dataset failed to capture the wind shift seen in Fig. 3b, requiring the use of the 32.4km resolution North American Regional Reanalysis (which did capture it) as the boundary condition (Mesinger et al. 2004). This in turn required the addition of a new outermost grid of 12.8km grid spacing, maintaining the 1/4 outer-to-inner ratio of grid spacing.

Another difference was in the vertical grid spacing. On Night 1, the lowest level is 30m deep, increasing 15% for each succeeding layer up to a maximum of 500m depth. On the more stable Night 2, the lowest level was set at 15m. This led to a change in the scheme the model used to calculate eddy diffusivity. On Night 1, the model is run on all grids with the Mellor-Yamada scheme (Mellor and Yamada 1974) to determine eddy diffusivities in the vertical (though these were not used in the simulation of tracer dispersion), with the Smagorinsky (1963) horizontal deformation scheme for the horizontal diffusion. The latter sets diffusion equal to 0.32 multiplied by the product of the horizontal deformation and the grid spacing. On Night 2, the Deardorff scheme (Deardorff

1980), by which a parameterized TKE is used to get the eddy diffusivities, proved superior. As grid spacing decreases, the Mellor-Yamada scheme becomes less appropriate as the resolved horizontal mixing increases (Zhong and Fast 2003), but both Mellor-Yamada and Deardorff have been applied at a grid spacing of 200m (Chan 2009; Chan 2010).

The simulation of a stable boundary layer at fine resolution is very difficult, with a large range of vertical profiles in models run with different schemes to parameterize eddy diffusion (Holtslag et al. 2013). This will likely lead to errors in the RAMS-simulated NBL, which will require the use of additional observed data in the dispersion simulation.

3.1.2 HYSPLIT

The HYSPLIT dispersion model (Draxler and Hess 1998) is applied to calculate the tracer concentration at each point in the domain, using the RAMS gridded meteorological data as input. This model has proven itself very useful for simulating airborne chemical transport from a source to a receptor location (e.g., Stunder et al. 2007), and is used here to reproduce the tracer transport from the various emission points to the SCT to be compared with the observed data. HYSPLIT is run by ingesting wind data and applying a known source term, and the resulting simulated concentration time series is then validated against the observed tracer data. Agreement between the simulated and observed concentrations provides confidence in the use of the coupled simulation to calculate the tracer budget.

HYSPLIT uses turbulence kinetic energy (TKE) to calculate a Gaussian distribution of turbulent wind values, which are randomly added to the mean wind values (taken from the 200m RAMS grid) to get the transport of each Lagrangian tracer particle. The TKE can be taken from RAMS, but the option also exists to apply a user-set value of TKE (possibly a variation on the RAMS values), and TKE is set to reproduce best the behavior of the NBL. As they are released into the atmosphere, the particles will begin as a concentrated cloud that gradually disperses as the particles are assigned different turbulent velocities.

3.2 Night 1 (11 to 12 May, 2009)

The model winds and temperature on the first night (Fig. 7, 8) approximate the observed winds at two levels at the tall tower. Temperatures agree to within about 1°C. Both levels experience a gradual cooling, with winds out of the northeast. Errors exist in upper level wind speeds (Fig. 8b), but the model captures well the wind shifts during the night (Figs. 7c, 8c), with errors usually less than 10°. At 34m, however, the RAMS wind speeds are often double the observed wind speeds (Fig. 7b).

The simulated PBL (Fig. 9a) compares well with the sodar (Fig. 4a), with winds out of the NE to ENE up to the tower level (Fig. 9a), with faster winds above 200m from 0000 UTC to 0400 UTC that decrease afterward. The simulated winds tend to be 1-2m/s too fast. Cooling at the surface occurs at a slow rate (Fig. 9b), precluding the formation of an inversion in the 0-350m range, with TKE remaining large (with a gradual decrease) within a deep layer (Fig. 9b). This has the effect of maintaining vertical turbulent transport (and preventing the LLJ from forming) throughout most of the night.

The meteorological variables from the RAMS simulation served as input to the HYSPLIT tracer model, and this is used to recreate what happened to the tracer that night. The release of tracer from the most distant point (WA) is simulated, using the known release rate (1906 g/hr), and the simulated concentration is compared with the observations at the tower at all three levels. The simulated surface plume is seen to begin as a thin stream emanating to the WSW from point WA, which then sweeps southward across the SCT at about 6:00am -7:00am EDT (1000-1100 UTC) as the wind becomes northerly (Fig. 10). The simulated plume does not sweep the tower at the correct time (Fig. 10b), however, arriving too late compared to the observations. To correct for this, the simulated tracer concentration is sampled at a point 5km to the north of the true tower location (Fig. 2), providing a vertical cross-section at the plume center. The vertical structure of the simulated plume corresponds well to the observed structure (Fig. 11a), with good agreement at all levels, suggesting that the too-fast wind speeds at low levels are not causing an unrealistic plume formation, and the model is simulating vertical turbulent transport with reasonable accuracy.

Next, a series of inverse transport simulations (i.e., running the model backward in time, or 'backtracking') is performed – releasing particles from the 329m level of the tower at various times. Thus, the particles move upwind while dispersing *downward*, eventually reaching the surface (unless they leave the innermost model domain before doing so). This pattern of particles within the surface layer constitutes the footprint – a measure of how strongly any area near the tower contributes to the tower signal. The more particles mix downward into a particular area, the more strongly that area influences the tower signal.

A large number of particles (100,000) was released from the 329m tower level on the Grid 3 domain as a single 'puff' each hour, and the fraction of these particles that diffuse into the surface layer (0 to 50m) within one hour in each model grid square constitutes the footprint (Fig. 12). On Night 1, the footprint lies to the northeast of the tower at all times, a consequence of the northeasterly wind (Fig. 9). Also, note that the footprint does not encompass the release points until about 0900 UTC as the winds shifts north. Toward the end of the period, the footprint is reduced (Fig. 12e, f) as the night becomes more stable (Fig. 1b, Fig. 9b), implying that the local influence becomes weaker. The fraction of released particles within the domain below 50m after one hour is plotted as a function of release time in Fig. 13a, and reflects the changes in Fig. 12 - relatively high nocturnal mixing early in the period gives way to reduced mixing by 6:00am to 8:00am EDT (1000 to 1200 UTC). In the "near-field" domain, the tower footprint tends to lie beyond 12km, and indicates a weak overall influence on the tower readings; only 2-5% of the particles have 'landed' within 20km of the tower, with about 80% having left the domain (Fig. 13b) in the one-hour period.

3.3 Night 2 (12 to 13 May, 2009)

On Night 2, the experiment began as the wind was out of the southeast (Fig. 3a), but swung around to the northeast during the night, providing an opportunity for the SCT to sample the plume. At 34m, the RAMS simulation captures well the wind shift and gradual rise in wind speed, as well as the gradual cooling trend (Fig. 14), though errors of about 1.5°C and 1.5m/s do exist, respectively. At 329m, however, the model has more difficulty with the wind speed (errors of about 3-5m/s), and underestimates the shift in direction (errors of about 20°) (Fig. 15). It does capture well the weaker

cooling trend at this upper level, setting up an inversion for the later portion of the night. The simulated PBL on this night (Fig. 16a) compares well to the observed (Fig. 4b), with a weak jet forming at 0300 UTC that fades before reforming at 0800 UTC. The model does miss the partially reformed jet at 0600 UTC, but overall the model is capturing the observed NBL behavior. In the model and the observations, this night more closely resembles a classic nocturnal PBL pattern – an inversion forming late in the night, with a strong LLJ forming above it and a turbulent layer near the surface (Fig. 16b). Winds accelerate as they shift from E to ENE (Figs. 4b, 16a).

Similar to Night 1, the HYSPLIT model is run for the tracer release from the most distant point – in this case, Point UE (Fig. 2), with PTCH as the PFC (Table 1) and a release rate of 396 g/hr. This simulation requires a change in the way the coupled model was run – in a preliminary simulation, the vertical diffusivity derived from the RAMS-simulated TKE (Fig. 16b) fails to mix the tracer upwards in the observed concentrations. To compensate for this, a subsequent simulation is run in which the TKE (seen in Fig. 16b) is multiplied by a factor of 5 to bring the simulation more into agreement with observations. The simulation produces a plume that sweeps the tower about one hour later than observed. If a sample point within the plume is selected and the time is adjusted by one hour, however, the model captures reasonably well the vertical cross-section of the tracer (Fig. 11b).

As for Night 1, 100,000 particles are released from the 329m level of the tower, and this is used to calculate the Night 2 footprint (Fig. 17). Early in the simulated period 2:00am to 3:00am EDT (0600 to 0700 UTC), the footprints indicate a local influence comparable to Night 1 (Fig. 17a, b), as the strongest inversion has not yet formed (Fig. 16b), in agreement with the low Ri values of Fig. 1b. After this time, however, limited vertical mixing above 50m is in evidence as the footprints (Fig. 17c-f) indicate a far weaker local influence on the tall tower compared to Night 1. When plotted as a function of release time (Fig. 13a), the calculated footprints are actually of larger magnitude compared to Night 1 for 2:00am to 3:00am EDT (0600 – 0700 UTC) during the early, less stable period, but soon after the local footprints become insignificant (the Night 2 bulk Ri values in Fig. 1b rise from 0600 UTC to 1100 UTC), indicating that the tower is sampling a more distant

part of the domain later in the night, with almost 100% of the particles leaving the domain after this time (Fig 13b).

4. Eddy Diffusivity

Turbulent transport in the atmosphere is often described with 'K-theory', in which the eddy flux is related to the vertical concentration gradient and an eddy diffusivity parameter (K_Z) (Stull 1988; Pasquill and Smith 1983). In this approach, the flux is related to both a source and a measure of turbulent transport:

$$\overline{w'c'} = -K_z \left(\frac{\partial \bar{c}}{\partial z}\right), \qquad 1$$

where $\overline{w'c'}$ is the vertical turbulent CO_2 flux and $\frac{\partial \bar{c}}{\partial z}$ is the vertical CO_2 gradient. The use of K-theory to parameterize an eddy flux using a resolved gradient is applied in many models, including that used by Carbon Tracker to produce a global carbon budget from the tall tower measurements (Peters et al. 2004; Krol et al. 2005), and it is a good indicator of turbulent transport (Sogachev and Leclerc 2011).

A time series of CO_2 concentrations on May 11th, 2009 at SRS (Fig. 18a) shows clearly the nocturnal increase at lower levels as respiring plants release CO_2 into the boundary layer, while values at the highest level (329m) show a decline, indicative of low-CO_2 advection or the removal of CO_2 out of the layer top by turbulence that exceeds the input rate at the bottom. Mixing exists between the lowest 2 levels, with small (but detectable) differences in concentration between them. After sunrise (~1030 UTC, 6:30am EDT), concentrations drop as plants start taking in CO_2 (Fig. 18a). Surface heating increases turbulent mixing, which tends to homogenize the boundary layer and reduce vertical gradients. On Night 2, evidence of nocturnal respiration also exists at lower levels (but with steady values at the highest level), with a turbulent mixing signal the following morning (Fig. 18a). Notice how weaker mixing exists between the lowest 2 levels on this more stable night.

Using data from the sonic anemometers and open-path infrared gas analyzers, the observed turbulent flux of CO_2 can be calculated as the covariance between vertical velocity and CO_2 concentration (as in Eq. 1), subject to the Webb-Pearman-Leuning (WPL) correction (Webb et al.

1980). The time series of perturbations was despiked (Vickers and Mahrt 1997), the wind components subjected to a planar fit coordinate rotation (Wilczak et al. 2001), and linearly detrended (Rannik and Vesala 1999).

Each sonic anemometer is placed on a boom extending from the tower at an angle pointing towards 208°. Given the locations of the tower supports, the tower structure will therefore affect winds from about 16° to 40°, and turbulent kinetic energy (TKE) and flux measurements will therefore be affected when the sensors are within the tower wake. On Night 1, the 68m wind was between 30° and 40° for about 1/3 of the night (from 0800 UTC to 1200 UTC), while that at 34m was within this range only about 15% of the night, never shifting north of 37° (Fig. 3a). (The Night 2 wind was never north of 40°.) The Night 1 friction velocity at all three levels (Fig. 19) does not show evidence of the introduction of a large amount of turbulence at 68m between 0830 UTC and 1200 UTC, as we would expect if the tower were generating a large amount of TKE. Therefore, no corresponding flux is eliminated in the analysis.

The nocturnal flux of CO_2 varies greatly during the night of May $11^{th}/12^{th}$. A time series of 30-minute averaged flux (Fig. 18b) clearly shows upward transport during most of the night, with brief periods of downward transport and at least one period of strong upward transport at 329m at about 10pm EDT (0200 UTC). The upward turbulent fluxes of CO_2 during night 2 (Fig. 18b) are on average lower than on Night 1.

We have concentration and flux data at 3 levels – 34m, 68m and 329m. The concentrations at 51m and 199m can be interpolated from the tower data. It is common to use resolved model data to parameterize the eddy diffusivity and calculate the turbulent fluxes. Because the fluxes and vertical gradients of CO_2 are both known, however, we can instead solve Eq. 1 for K_Z directly and characterize the magnitude of turbulent transport during this experimental period.

On Night 1, K_Z reaches higher values in the lower layer (Fig. 20a) than the upper layer (Fig. 20a), as vertical eddy transport is maintained despite a weak vertical gradient (Fig. 18a). In the upper layer (Fig. 20a), a decrease in turbulent mixing can be seen after 0700 UTC, consistent with the gradual stabilization of the Night 1 NBL inferred from the bulk Ri value (Fig. 1b), the footprint (Fig. 12), and the simulated TKE (Fig. 9b). The higher K_z values at both levels are also consistent

with periods of strong mixing inferred from the Night 1 tracer time series (Fig. 5a, b). On Night 2, the inferred K_Z values are an order of magnitude smaller than for Night 1 (Fig. 20a, b), again indicating greater stability on this night. Note that the K_Z values on Night 2 are larger at upper levels, in the area beneath the LLJ.

5. Discussion and Conclusions

We can draw three conclusions from this experiment:

i) A local signal observed at the SCT as a tracer released within the tower vicinity was detected at the uppermost sensor (329m), indicating that, even in stable and slightly stable conditions, sufficient vertical mixing exists to move tracer from the surface to this level within ~25 km. This implies that the tracer was able to penetrate above the boundary layer top and that stable or slightly stable nocturnal conditions do not necessarily confine gases released at the surface within a shallow layer.

ii) A fetch of 4-25km in length is adequate for a tracer to be mixed upwards to 329m, a level typical of a 'tall' sampling tower. This indicates that such a tower is at least partly influenced by the local landscape during a time when it is assumed to be sampling continental-scale air masses.

iii) The simulation of the tracer release shows how the tower footprints vary with stability, as the local-scale footprint tends to disappear as the PBL becomes more stable. In both cases, the local influence is small, with most of the released particles leaving the domain (~20km) within a short time. This suggests that the boundary layer height in Fig. 1c can be considered as a 'leaky' barrier to upward diffusion, confining most of the tracer released beneath it. This is similar to the conclusion from Sogachev and Leclerc (2011), in which calculated tower footprints in stable conditions often lay entirely beyond 50km of the tower, indicating that the tower is predominately sampling areas hundreds of kilometers from the tower.

Confidence in the results based on a simulation is of course limited by the quality of the simulation. Our simulation of the boundary layer on the two nights is in general agreement with the observed boundary layer, and errors in the simulated winds do lead to problems in the simulated plumes. On both nights, the plumes seem to form properly but not move as observed. Because the

simulated concentrations at the different tower levels are in (again, rough) agreement with the observed values, however, the simulated vertical diffusion results are likely to be correct, and the simulated footprints represent well the influence of the surrounding area on the tower. This conclusion is strengthened by the agreement between the simulated footprint behavior and the observed measures of stability and vertical transport.

Independent of the artificial tracer release, the CO_2 concentration and flux time series also reflect the changes in stability on vertical transport on the two nights – nocturnal respiration increases CO_2 values in the boundary layer, with greater vertical gradients of CO_2 on the more stable night. Greater turbulent mixing (as quantified by eddy diffusivity) is observed during the night characterized by lower stability. The tracer data, the simulated tracer release, and the calculated eddy diffusivities all agree in that they indicate a stronger local influence on Night 1 than on Night 2.

This study has implications beyond a single tower. Our results speak to the importance of vertical transport on the calculation of a global carbon budget constrained with limited carbon measurements. The SCT is a component of NOAA's 'tall tower' network, which measures carbon concentrations to quantify the terms of the carbon budget, especially those dealing with the land surface (Birdsey et al. 2009; Stephens et al. 2007; Gourdji et al. 2012). Terrestrial ecosystems constitute a major sink of carbon, but their magnitude is uncertain (Birdsey et al. 2009). NOAA initiated the Carbon Tracker project to process global carbon measurements and produce a complete global carbon budget (Peters et al. 2007). The network is currently active in making measurements (Andrews et al. 2013), and this monitoring resource forms the North American backbone of the Carbon Tracker project.

Gerbig et al. (2009) discusses that errors in the parameterized vertical transport in transport models used for top-down inversions can produce errors in the reconstructed global emissions. Peters et al. (2004) demonstrated errors in the global budget of an artificial tracer (SF6), and attributed some of them to problems with the calculation of vertical eddy diffusivity in the TM5 transport model, the same model used to get the global carbon inversion. Gerbig et al. (2009) also suggest 'adding Lidar measurements to monitor mixing heights at the tall tower locations, which when assimilated into the meteorological transport fields are likely to improve the representation of

the measurements'. In the absence of such measurements, numerical modeling can serve as a good proxy for the determination of mixing parameters.

We acknowledge that an extension of these results is limited and that further work is needed for a more comprehensive footprint assessment from tall towers in a wide variety of stability conditions. The influence of the local environment is related to both vertical mixing and advection, and weaker advection of air from distant sources could make the local influence stronger than was seen during the nights of the tracer release. The local effect must be considered when data from a tall tower is being evaluated.

6. Acknowledgements

This document was prepared in conjunction with work accomplished under Contract No. DE-AC09-08SR22470 with the U.S. Department of Energy. Funding was provided by the DOE Office of Science – Terrestrial Carbon Processes program. The authors would like to thank the following individuals for assisting with the field studies. David Durden, Natchaya Pingintha and Natthaphol Lichaikul from the University of Georgia, Keith Lewin, Rick Wilke, Larry Milian, Scott Smith, John Heiser, and Jay Adams from Brookhaven National Laboratory, John T. Hamilton, Jr, and Ronald W. Johnson from the Savannah River National Laboratory, Arlyn Andrews, Jonathan Kofler and Jonathan Williams from the NOAA-Global Monitoring Division, Erik Kabela, now with the Oak Ridge National Laboratory, and Borja Ruiz Reverter from Grupo de Física de la Atmósfera, Centro Andaluz de Medio Ambiente (CEAMA) Universidad de Granada, Granada, Spain.

7. References

Andrews A, Kofler J, Trudeau M, Williams J, Neff D, Masarie K, Chao D, Kitzis D, Novelli P, Zhao C, Dlugokencky E, Lang P, Crotwell M, Fischer M, Parker M, Lee J, Baumann D, Desai A, Stanier C, de Wekker S, Wolfe D, Munger J, Tans P (2013) CO_2, CO and CH_4 Measurements from the NOAA Earth System Research Laboratory's Tall Tower Greenhouse Gas Observing Network: instrumentation, uncertainty analysis and recommendations for future high-accuracy greenhouse gas monitoring efforts. Atmospheric Measurement Techniques, 6:1461-1553.

Barcza Z., Kern A, Haszpra L, Kljun N (2009) Spatial representativeness of tall tower eddy covariance measurements using remote sensing and footprint analysis. Ag For Met 149:795–807

Barkhatov Y, Belolipetsky P, Degermendzhi A, Belolipetskii V, Verkhovets S, Timokhina A, Panov A, Schhemel A, Vedrova E, and Trephilova O (2012) Modeling of CO_2 fluxes between atmosphere and boreal forest. Procedia Environmental Sciences 13:621-625.

Benjamin S, Dévényi D, Weygandt S, Brundage K, Brown J, Grell G, Kim D, Schwartz B, Smirnova T, Smith T, Manikin G (2004) An Hourly Assimilation–Forecast Cycle: The RUC. Mon. Wea. Rev. 132:495–518.

Birdsey R, Bates N, Behrenfeld M, Davis K, Doney S, Feely R, Hansell D, Heath L, Kasischke E, Khesghi H, Law B, Lee C, McGuire A, Raymond P, Tucker C (2009) Carbon cycle observations: gaps threaten climate mitigation policies. Eos, 90(34):292-293.

Cai X, Peng G, Guo X, Leclerc M (2008) Evaluation of backward and forward Lagrangian footprint models in the surface layer. Theor. Appl. Clim., 93, 207-223, doi: 10.1007/s00704-007-0334-0

Chan P (2009) Atmospheric turbulence in complex terrain: Verifying numerical model results with observations by remote-sensing instruments. Meteor. and Atmos. Phys. 103:145-157.

Chan P (2010) Validating the turbulence parameterization schemes of a numerical model using eddy dissipation rate and turbulent kinetic energy measurements in terrain-disrupted airflow. Meteor. and Atmos. Phys. 108:95-112.

Chen B, Coops N, Fu D, Margolis H, Amiro B, Black T, Arain M, Barr A, Bourque C, Flanagan L, Lafleur P, McCaughey J, Wofsy S (2012) Characterizing spatial representativeness of

flux tower eddy-covariance measurements across the Canadian Carbon Program Network using remote sensing and footprint analysis. Remote Sensing of Environment 124:742–755

Chen B, Zhang H, Coops N, Fu D, Worthy D, Xu G, Black T (2013) Assessing scalar concentration footprint climatology and land surface impacts on tall-tower CO_2 concentration measurements in the boreal forest of central Saskatchewan, Canada. Theor. Appl. Clim. doi: 10.1007/s00704-013-1038-2

Clark T, Hall W (1991) Multi-domain simulations of the time dependent Navier-Stokes equations: Benchmark error analysis of some nesting procedures. J. Comput. Phys. 92:456-481.

Cotton W, Tripoli G, Rauber R, Mulvihill E (1986) Numerical simulation of the effects of varying ice crystal nucleation rates and aggregation processes on orographic snowfall. J. Climate Appl. Meteor. 25:1658-1680.

Deardorff J (1980) Stratocumulus-capped mixed layers derived from a three-dimensional model. Bound. Lay. Met. 18:495-527.

Desai A, Noormets A, Bolstad P, Chen J, Cook B, Davis K, Euskirchen E, Gough C, Martin J, Ricciuto D, Schmid H, Tang J, Wang W (2008) Influence of vegetation and seasonal forcing on carbon dioxide fluxes across the Upper Midwest, USA: Implications for regional scaling. Ag. For. Met. 148:288-308

Draxler R, Hess G (1998) An overview of the HYSPLIT_4 modeling system of trajectories, dispersion, and deposition. Aust. Meteor. Mag. 47:295-308.

Gerbig C, Dolman A, Heimann M (2009) On observational and modelling strategies targeted at regional carbon exchange over continents. Biogeosciences, 6:1949-1959, doi:10.5194/bg-6-1949-2009

Gloor M, Bakwin P, Hurst D, Lock L, Draxler R, Tans P (2001) What is the concentration footprint of a tall tower? J. Geophys. Res. 106:17831-17840

Gourdji S, Mueller K, Yadav V, Huntzinger D, Andrews A, Trudeau M, Petron G, Nehrkorn T, Eluszkiewicz J, Henderson J, Wen D, Lin J, Fischer M, Sweeney C, Michalak A (2012) North American CO_2 exchange: inter-comparison of modeled estimates with results from a fine-scale atmospheric inversion. Biogeosciences 9:457-475, doi:10.5194/bg-9-457-2012

Harrington J (1997) The effects of radiative and microphysical processes on simulated warm transition season Arctic stratus, Dept. of Atmospheric Science Bluebook 637, Colorado State University, Fort Collins, CO, 289 pp.

Hegarty, J, and Coauthors (2013) Evaluation of Lagrangian particle dispersion models with measurements from controlled tracer releases. J. Appl. Meteor. Climatol. 52:2623–2637. doi: http://dx.doi.org/10.1175/JAMC-D-13-0125.1

Holtslag A, and Coauthors (2013) Stable Atmospheric Boundary Layers and Diurnal Cycles: Challenges for Weather and Climate Models. Bull. Amer. Meteor. Soc. 94:1691–1706.

Krol M, Houweling S, Bregman B, nan den Broek M, Segers A, van Velthoven P, Peters W, Dentener F, Bergamaschi P (2005) The two-way nested global chemistry-transport zoom model TM5: algorithm and applications. Atmos. Chem. Phys. 5:417-432

Kuo H (1974) Further studies of the parameterization of the influence of cumulus convection on large-scale flow. J. Atmos. Sci. 31:1232-1240.

Leclerc M, Karipot A, Prabha T, Allwine G, Lamb B, Gholz H (2003a) Impact of non-local advection on flux footprints over a tall forest canopy: a tracer flux experiment. Ag. For. Met. 115:19-30.

Leclerc M, Meskhidze N, Finn D. (2003b) Comparison between measured tracer fluxes and footprint model predictions over a homogeneous canopy of intermediate roughness. Ag. For. Met. 117:145-158.

Leclerc M, Thurtell G (1990) Footprint predictions of scalar fluxes using a Markovian analysis. Bound.-Layer Meteorol. 52:247–258.

Mellor G, Yamada T (1974) A hierarchy of closure models for planetary boundary layers. J. Atmos. Sci., 31:1791-1806.

Mesinger F, Arakawa A (1976) Numerical methods used atmospheric models. GARP Publication Series, No. 14, WMO/ICSU Joint Organizing Committee, 64pp.

Mesinger F, DiMego G, Kalnay E, Shafran P, Ebisuzaki W, Jovic D, Woollen J, Mitchell K, Rogers E, Ek M, Fan Y, Grumbine R, Higgins W, Li H, Lin Y, Manikin G, Parrish D, Shi W (2004) North American Regional Reanalysis. 15th Symposium on Global Change and Climate Variations,

paper P1.1, Combined Preprints CD-ROM, 84th AMS Annual Meeting, Seattle, WA. Updated 31 December 2003.

Meyers M, DeMott P, Cotton W (1992) New primary ice nucleation parameterizations in an explicit cloud model. J. Appl. Meteor. 31:708-721.

Pasquill F, Smith F (1983) Atmospheric Diffusion, John Wiley and Sons, NY

Peters W, Jacobson A, Sweeney C, Andrews A, Conway T, Masarie K, Miller J, Bruhwiler L, Pétron G, Hirsch A, Worthy D, van der Werf G, Randerson J, Wennberg P, Krol M, Tans P (2007) An atmospheric perspective on North American carbon dioxide exchange: CarbonTracker, Proceedings of the National Academy of Sciences of the United States of America, 104, n. 48:18925–18930, doi:http://dx.doi.org/10.1073/pnas.0708986104

Peters W, Krol M, Dlugokencky E, Dentener F, Bergamaschi P, Dutton G, Velthoven P, Miller J, Bruhwiler L, Tans P (2004) Toward regional-scale modeling using the two-way nested global model TM5: Characterization of transport using SF_6. J. Geophys. Res. 109, D19314, doi:10.1029/2004JD005020.

Pielke R, Cotton W, Walko R, Tremback C, Lyons W, Grasso L, Nicholls M, Moran M, Wesley D, Lee T, Copeland J (1992) A comprehensive meteorological modeling system-RAMS. Meteor. Atmos. Phys. 49:69-91.

Rannik Ü, Markkanen T, Raittila J, Hari P, Vesala T (2003) Turbulence statistics inside and over forest: Influence on Footprint Prediction. Bound-Layer Meteor 109:163-189.

Rannik Ü, Vesala T (1999) Autoregressive filtering versus linear detrending in estimation of fluxes by the eddy covariance method. Bound-Layer Meteor, 91:259 – 280

Schuepp P, Leclerc M, MacPherson J, Desjardins R (1990) Footprint prediction of scalar fluxes from analytical solutions of the diffusion equation. Bound. Lay. Met. 50:355-373.

Smagorinsky J (1963) General circulation experiments with the primitive equations. Part I, The basic experiment. Mon. Wea. Rev. 91:99-164.

Sogachev A, Leclerc M (2011) On concentration footprints for a tall tower in the presence of a nocturnal low-level jet, Ag. For. Met. 151:755-764.

Sogachev A, Panferov O, Gravenhorst G, Vesala T (2005) Numerical analysis of flux footprints for different landscapes, Theor. Appl. Clim., 80, 169-185, doi: 10.1007/s00704-004-0098-8

Stephens B, Gurney K, Tans P, Sweeney C, Peters W, Bruhwiler L, Ciais P, Ramonet M, Bousquet P, Nakazawa T, Aoki S, Machida T, Inoue G, Vinnichenko N, Lloyd J, Jordan A, Heimann M, Shibistova O, Langenfelds R, Steele L, Francey R, Denning A (2007) Weak Northern and Strong Tropical Land Carbon Uptake from Vertical Profiles of Atmospheric CO_2. Science, 316 no. 5832:1732-1735. DOI: 10.1126/science.1137004

Stull R (1988) An introduction to boundary layer meteorology. Kluwer, 666 pp.

Stunder B, Heffter J, Draxler R (2007) Airborne Volcanic Ash Forecast Area Reliability. Wea. Forecasting 22:1132–1139.

van Dop H, Addis R, Fraser G, Girardi F, Graziani G, Inoue Y, Kelly N, Klug W, Kulmala A, Nodop K, Pretel J (1998) ETEX: A European tracer experiment; observations, dispersion modelling and emergency response. Atmos. Env. 32:4089-4094.

Vickers D, Mahrt L (1997) Quality control and flux sampling problems for tower and aircraft data. J Atmos Ocean Tech, 14:512 – 526.

Walko R, Band L, Baron J, Kittel T, Lammers R, Lee T, Ojima D, Pielke R, Taylor C, Tague C, Tremback C, Vidale P (2000) Coupled Atmosphere–Biophysics–Hydrology Models for Environmental Modeling. J. Appl. Meteor. 39:931–944.

Wang W, Davis K, Cook B, Yi C, Butler M, Ricciuto D, Bakwin P (2007) Estimating daytime CO2 fluxes over a mixed forest from tall tower mixing ratio measurements, J. Geophys Res. V112, 2006JD007770

Webb E, Pearman G, Leuning R (1980) Correction of the flux measurements for density effects due to heat and water vapour transfer. Q J R Meteorol Soc, 106:85–100.

Werth D, Kurzeja R, Luís Dias N, Zhang G, Duarte H, Fischer M, Parker M, Leclerc M (2011) The Simulation of the Southern Great Plains Nocturnal Boundary Layer and the Low-Level Jet with a High-Resolution Mesoscale Atmospheric Model. J. Appl. Meteor. Climatol., 50:1497–1513.

Wilczak J, Oncley S, Stage S (2001) Sonic anemometer tilt correction algorithms. Bound-Layer Meteor. 99:127 – 150.

Zhong S, Fast J (2003) An Evaluation of the MM5, RAMS, and Meso-Eta Models at Subkilometer Resolution Using VTMX Field Campaign Data in the Salt Lake Valley. Mon. Wea. Rev. 131:1301–1322.

Figure Captions

Fig. 1 a) Radio Acoustic Sounding System (RASS) temperature sounding at 2:00am EDT (0600 UTC) for (left) May 11/12th [Night 1], (right) May 12/13th [Night 2], b) as in a) but for the time series of bulk Ri calculated between 68m and 329m. c) LIDAR Ceiliometer readings of the boundary layer height for both nights. The straight black line is at 329m.

Fig. 2 Map of numbered tracer release points (red), as well as the tower receptor (black). Table 1 shows which tracer was released from which point for each night. Topographic heights range from 30m above ground level (darkest shading) to 150m (lightest shading). The RASS is co-located with release point 10.

Fig. 3 Wind direction (degrees) at Tall Tower on a) Night 1 and b) Night 2.

Fig. 4 Remtech sodar profile of the NBL wind speed and direction on a) Night1, and b) Night 2.

Fig. 5 Observed tracer for a) PMCH, Night 1, b) PTCH Night 1, c) PDCB, Night 2, d) PTCH, Night 2.

Fig. 6 Topography (m) for a) Grids 1 and 2, and b) Grid 3. The star indicates the tower location.

Fig. 7 Comparison of RAMS data (solid line) with observed tower data (dashed line) for Night 1 at 34m for a) temperature, b) wind speed, and c) wind direction.

Fig. 8 As in Fig. 7 but at 329m.

Fig. 9 a) Simulated Night 1 wind vectors and speeds (m/s) at the center of the innermost domain. b) As in a), but for temperature (shaded, degrees C) and TKE (m^2/s^2).

Fig. 10 Simulated Night 1 concentration within the 0-50m layer at a) 0700 UTC, b) 0900 UTC, and c) 1100 UTC. The large black dot represents the tall tower position.

Fig. 11 a) Time series of simulated and observed concentrations of tracer PTCH, emitted from Pt. WA, on Night 1. b) Time series of simulated and observed concentrations of tracer PTCH, emitted from Pt. UE, on Night 2. The 'tower' is actually shifted 5km north on Night 1 and 10km on Night 2, and the simulated data are time shifted by 1 hour on Night 2.

Fig. 12 Simulated Night 1 footprint at landing time a) 0600 UTC, b) 0700 UTC, c) 0800 UTC, d) 0900UTC, e) 1000 UTC, and f) 1100 UTC. Units represent fraction of released particles per square meter x 10^{-9}, and the dot represents the location of the tall tower.

Fig. 13 a) Fraction of particles that diffuse to within 50m of the surface in 1 hour as a function of landing time, b) as in a, but for the fraction of particles that have left the innermost domain after 1 hour.

Fig. 14 Comparison of RAMS data (solid line) with observed tower data (dashed line) for Night 2 at 34m for a) temperature, b) wind speed, and c) wind direction.

Fig. 15 As in Fig. 14 but at 329m.

Fig. 16 As in Fig. 9, but for Night 2.

Fig. 17 As in Fig. 12 but for Night 2.

Fig. 18 a) CO_2 concentrations and b) vertical CO_2 fluxes at the Tall Tower on Night 1 (left), and Night 2 (right).

Fig. 19 Night 1 friction velocity at the three tower levels.

Fig. 20 a) Turbulent Mixing eddy diffusivity (K) value on Night 1 at 51m and 199m, as calculated with the observed flux and gradient. b) As in a), but for Night 2.

Table 1 Tracer assigned to each location in Fig. 1. Note that Point 8 was never assigned.

Table 2 Release rates of the various tracers on both nights.

Figure

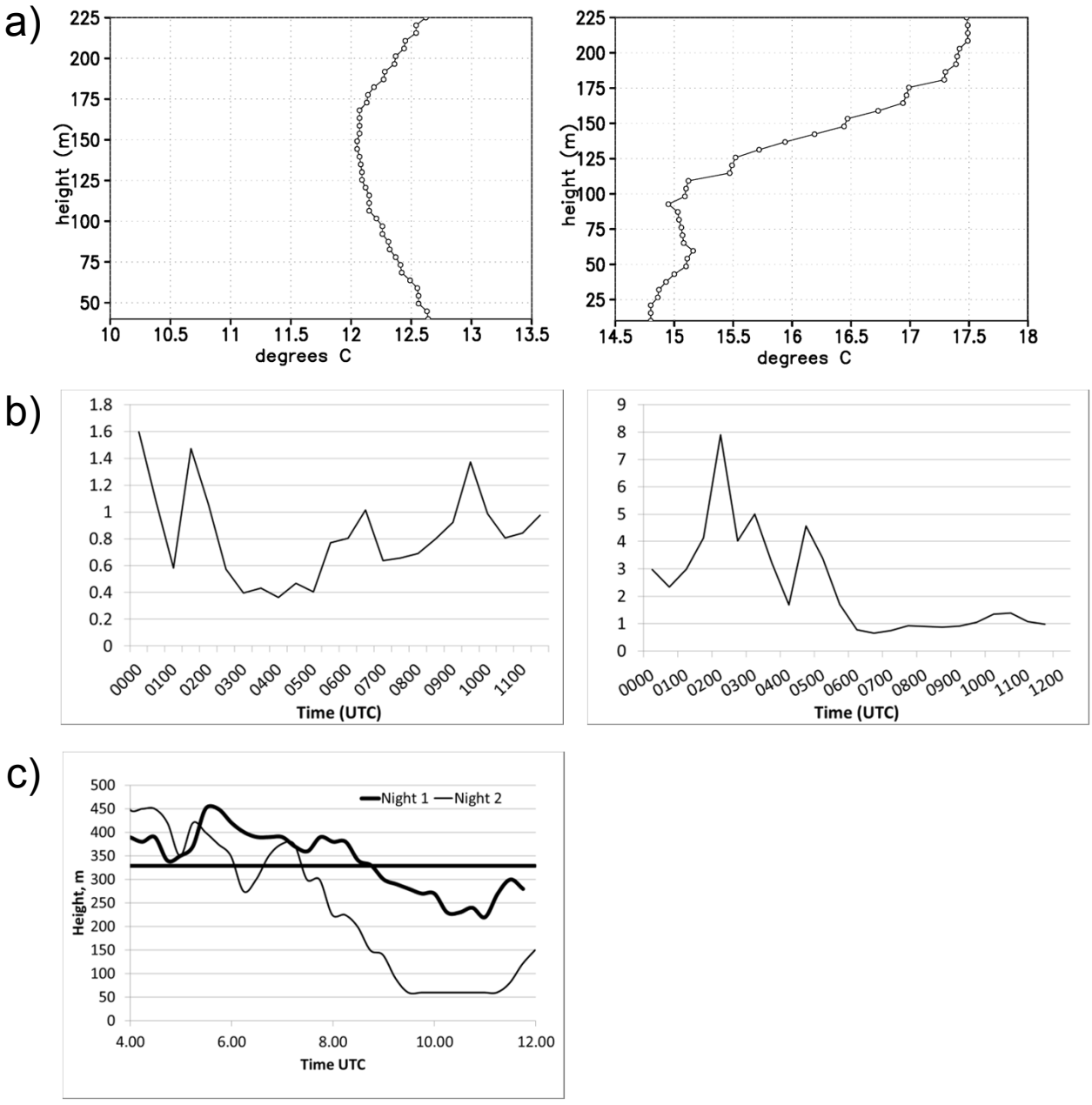
a)
height (m)
degrees C
b)
Time (UTC)
c)
Night 1
Night 2
Height, m
Time UTC

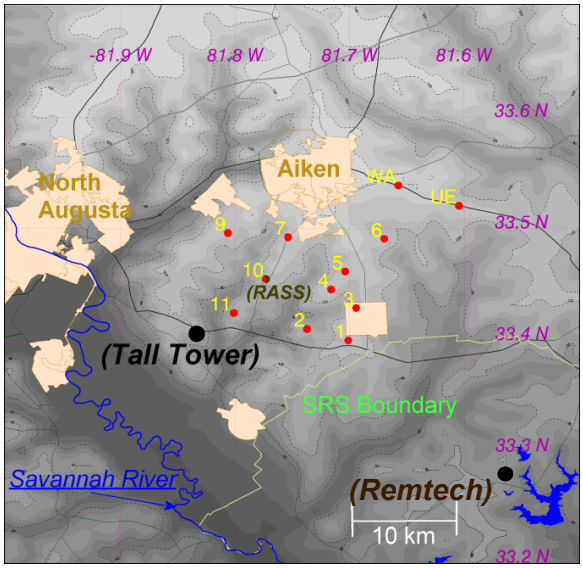
-81.9 W
81.8 W
81.7 W
81.6 W
33.6 N
33.5 N
33.4 N
33.3 N
33.2 N
Aiken
North
Augusta
WA
UF
9
7
6
10
(RASS)
5
4
3
11
2
1
(Tall Tower)
SRS Boundary
Savannah River
(Remtech)
10 km

a)

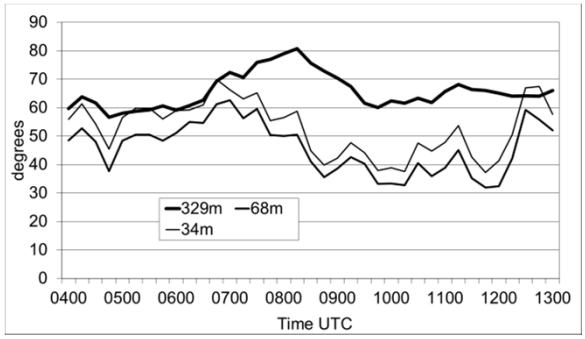
90
80
70
60
50
40
30
20
10
0
degrees
329m
68m
34m
0400
0500
0600
0700
0800
0900
1000
1100
1200
1300
Time UTC

b)

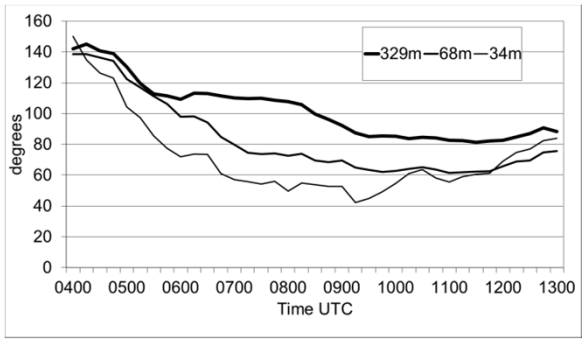
160
140
120
100
80
60
40
20
0
degrees
329m
68m
34m
0400
0500
0600
0700
0800
0900
1000
1100
1200
1300
Time UTC

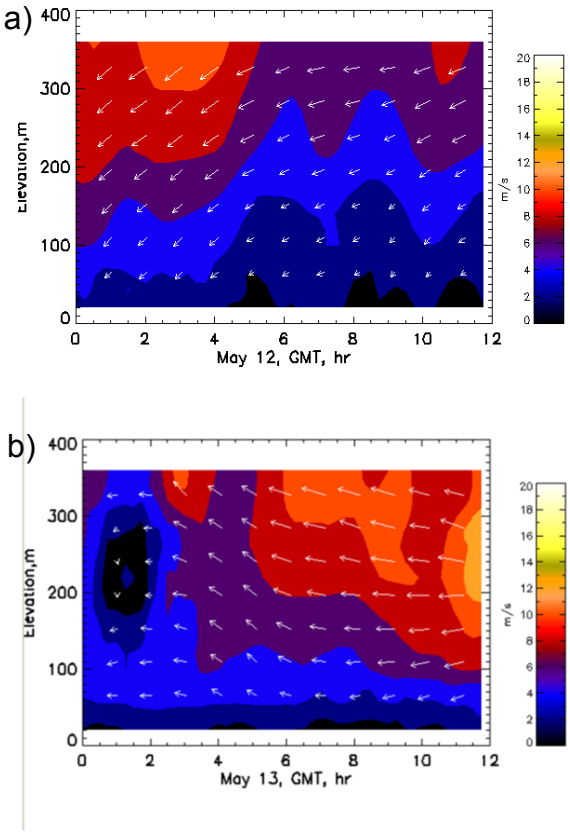
a)
400
300
200
100
0
Elevation,m
0
2
4
6
8
10
12
May 12, GMT, hr
20
18
16
14
12
10
8
6
4
2
0
m/s
b)
400
300
200
100
0
Elevation,m
0
2
4
6
8
10
12
May 13, GMT, hr
20
18
16
14
12
10
8
6
4
2
0
m/s

a)

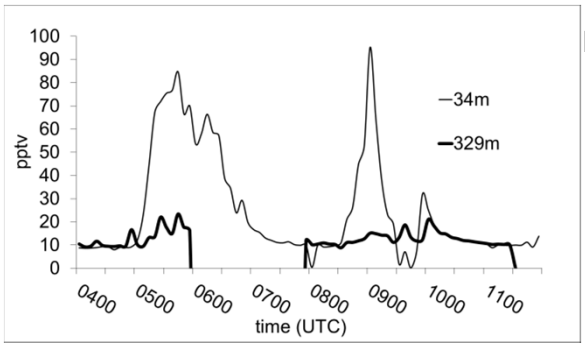
100
90
80
70
60
50
40
30
20
10
0
pptv
—34m
—329m
0400
0500
0600
0700
0800
0900
1000
1100
time (UTC)

b)

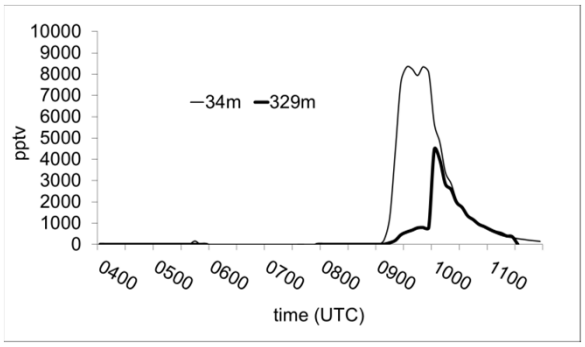
10000
9000
8000
7000
6000
5000
4000
3000
2000
1000
0
pptv
—34m —329m
0400
0500
0600
0700
0800
0900
1000
1100
time (UTC)

c)

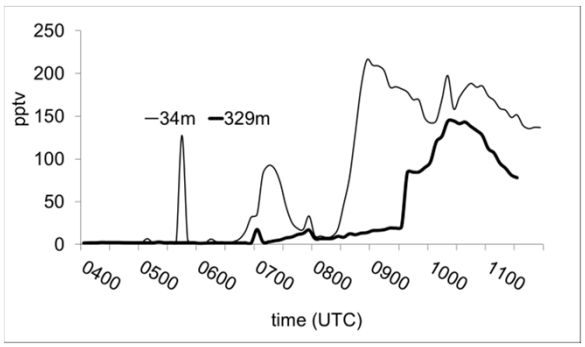
250
200
150
100
50
0
pptv
—34m —329m
0400
0500
0600
0700
0800
0900
1000
1100
time (UTC)

d)

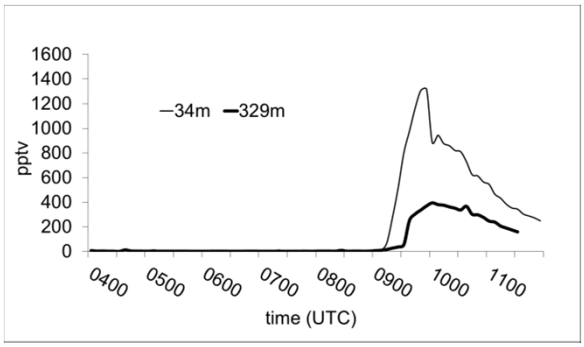
1600
1400
1200
1000
800
600
400
200
0
pptv
—34m —329m
0400
0500
0600
0700
0800
0900
1000
1100
time (UTC)

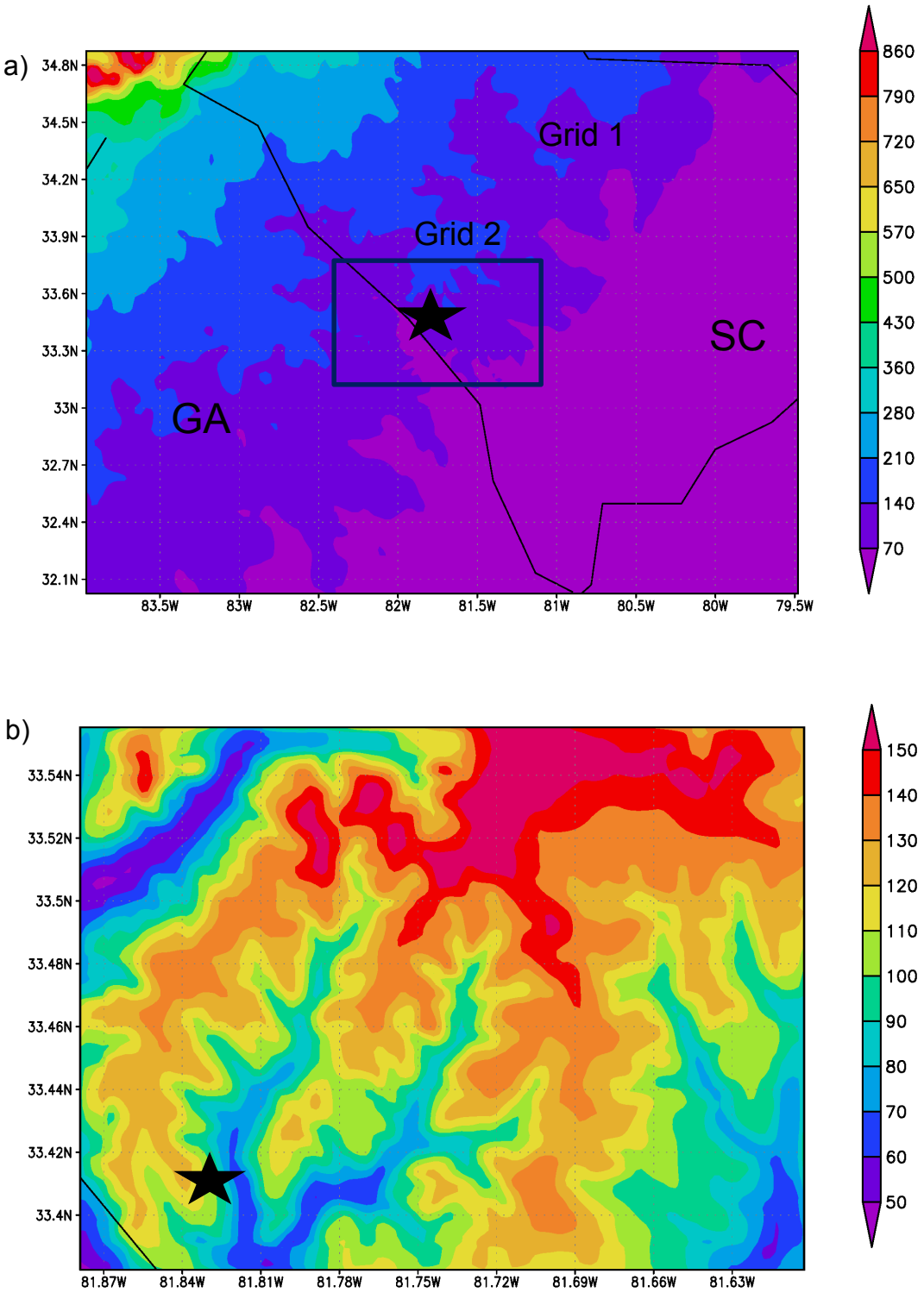
a)
34.8N
34.5N
34.2N
33.9N
33.6N
33.3N
33N
32.7N
32.4N
32.1N
83.5W
83W
82.5W
82W
81.5W
81W
80.5W
80W
79.5W
Grid 1
Grid 2
SC
GA
860
790
720
650
570
500
430
360
280
210
140
70
b)
33.54N
33.52N
33.5N
33.48N
33.46N
33.44N
33.42N
33.4N
81.87W
81.84W
81.81W
81.78W
81.75W
81.72W
81.69W
81.66W
81.63W
150
140
130
120
110
100
90
80
70
60
50

a)

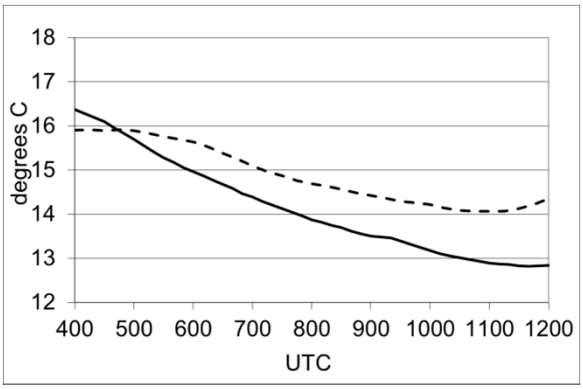
18
17
16
15
14
13
12
degrees C
400 500 600 700 800 900 1000 1100 1200
UTC

b)

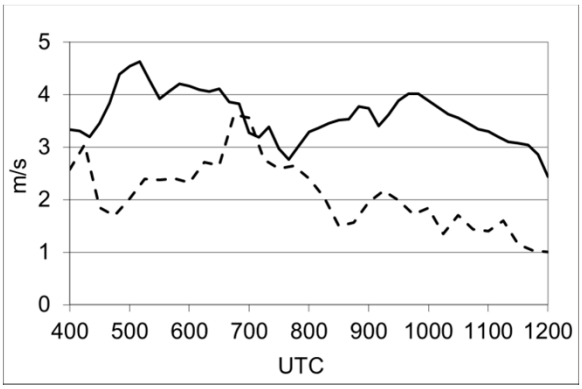
5
4
3
2
1
0
m/s
400 500 600 700 800 900 1000 1100 1200
UTC

c)

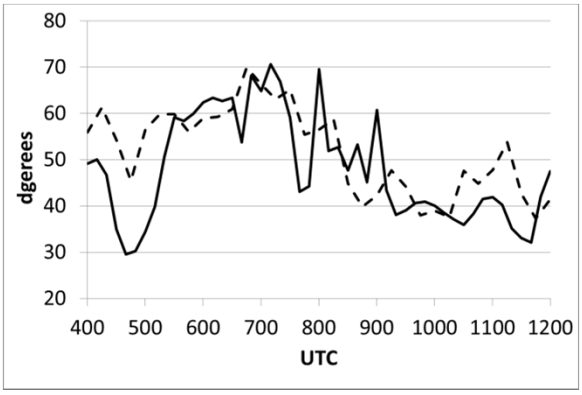
80
70
60
50
40
30
20
dgerees
400 500 600 700 800 900 1000 1100 1200
UTC

a)

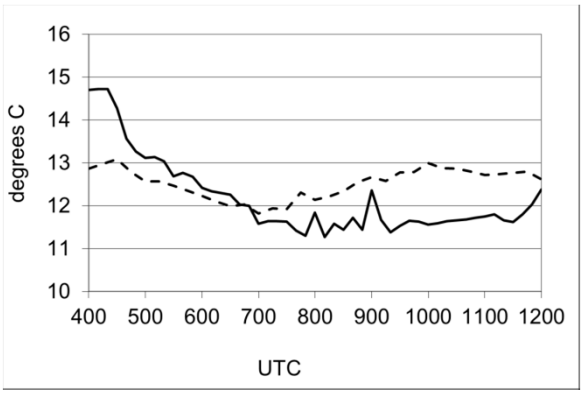
16
15
14
13
12
11
10
degrees C
400 500 600 700 800 900 1000 1100 1200
UTC

b)

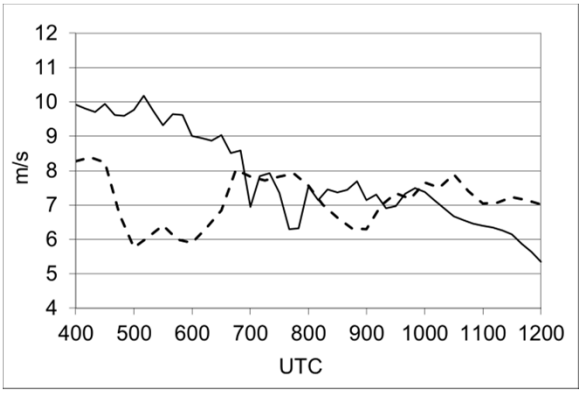
12
11
10
9
8
7
6
5
4
m/s
400 500 600 700 800 900 1000 1100 1200
UTC

c)

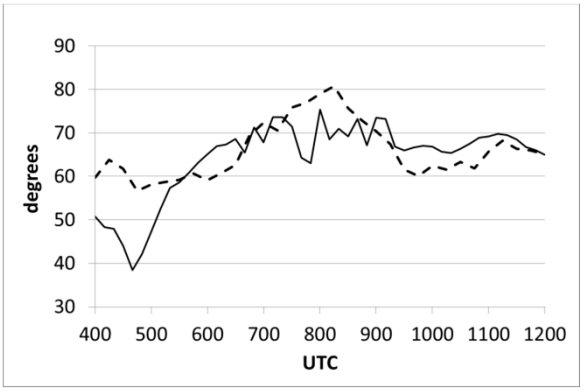
90
80
70
60
50
40
30
degrees
400 500 600 700 800 900 1000 1100 1200
UTC

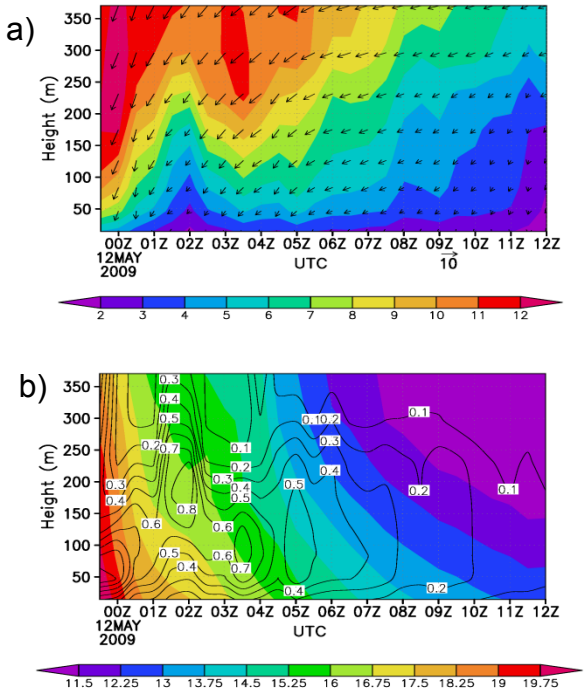
a)
Height (m)
350
300
250
200
150
100
50
00Z 01Z 02Z 03Z 04Z 05Z 06Z 07Z 08Z 09Z 10Z 11Z 12Z
12MAY
2009
UTC
$\overrightarrow{10}$
2 3 4 5 6 7 8 9 10 11 12
b)
Height (m)
350
300
250
200
150
100
50
00Z 01Z 02Z 03Z 04Z 05Z 06Z 07Z 08Z 09Z 10Z 11Z 12Z
12MAY
2009
UTC
11.5 12.25 13 13.75 14.5 15.25 16 16.75 17.5 18.25 19 19.75

a)

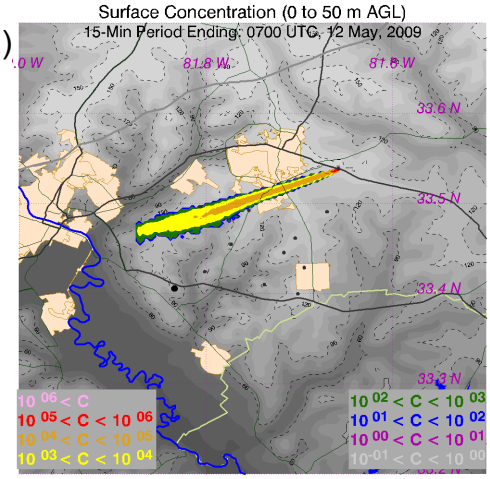
Surface Concentration (0 to 50 m AGL)
15-Min Period Ending: 0700 UTC, 12 May, 2009
81.8 W
81.6 W
33.6 N
33.5 N
33.4 N
33.3 N
10 06 < C
10 05 < C < 10 06
10 04 < C < 10 05
10 03 < C < 10 04
10 02 < C < 10 03
10 01 < C < 10 02
10 00 < C < 10 01
10-01 < C < 10 00

b)

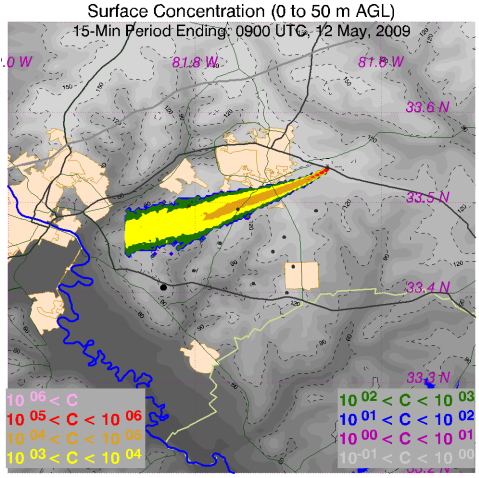
Surface Concentration (0 to 50 m AGL)
15-Min Period Ending: 0900 UTC, 12 May, 2009
81.8 W
81.6 W
33.6 N
33.5 N
33.4 N
33.3 N
10 06 < C
10 05 < C < 10 06
10 04 < C < 10 05
10 03 < C < 10 04
10 02 < C < 10 03
10 01 < C < 10 02
10 00 < C < 10 01
10-01 < C < 10 00

c)

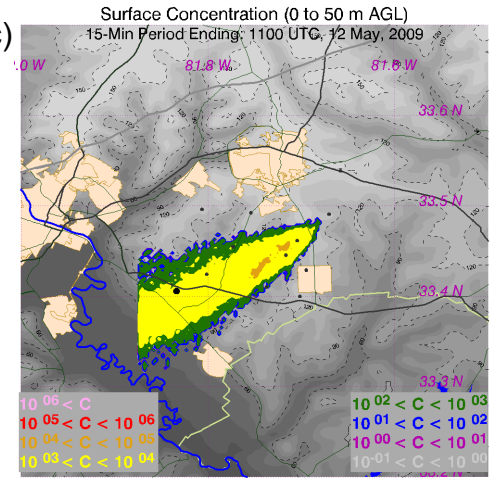
Surface Concentration (0 to 50 m AGL)
15-Min Period Ending: 1100 UTC, 12 May, 2009
81.8 W
81.6 W
33.6 N
33.5 N
33.4 N
33.3 N
10 06 < C
10 05 < C < 10 06
10 04 < C < 10 05
10 03 < C < 10 04
10 02 < C < 10 03
10 01 < C < 10 02
10 00 < C < 10 01
10-01 < C < 10 00

a)

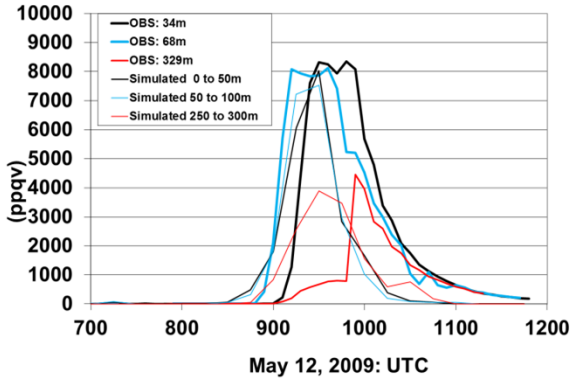
OBS: 34m
OBS: 68m
OBS: 329m
Simulated 0 to 50m
Simulated 50 to 100m
Simulated 250 to 300m
(ppqv)
10000
9000
8000
7000
6000
5000
4000
3000
2000
1000
0
700
800
900
1000
1100
1200
May 12, 2009: UTC

b)

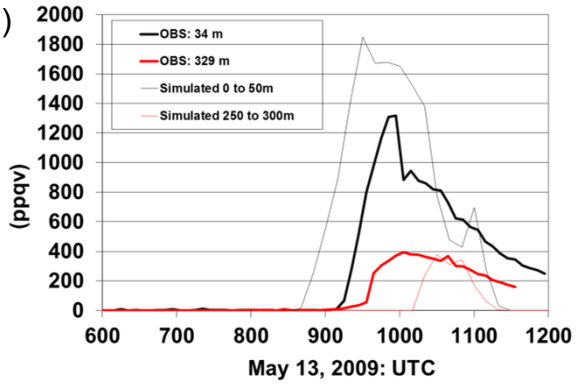
OBS: 34 m
OBS: 329 m
Simulated 0 to 50m
Simulated 250 to 300m
(ppqv)
2000
1800
1600
1400
1200
1000
800
600
400
200
0
600
700
800
900
1000
1100
1200
May 13, 2009: UTC

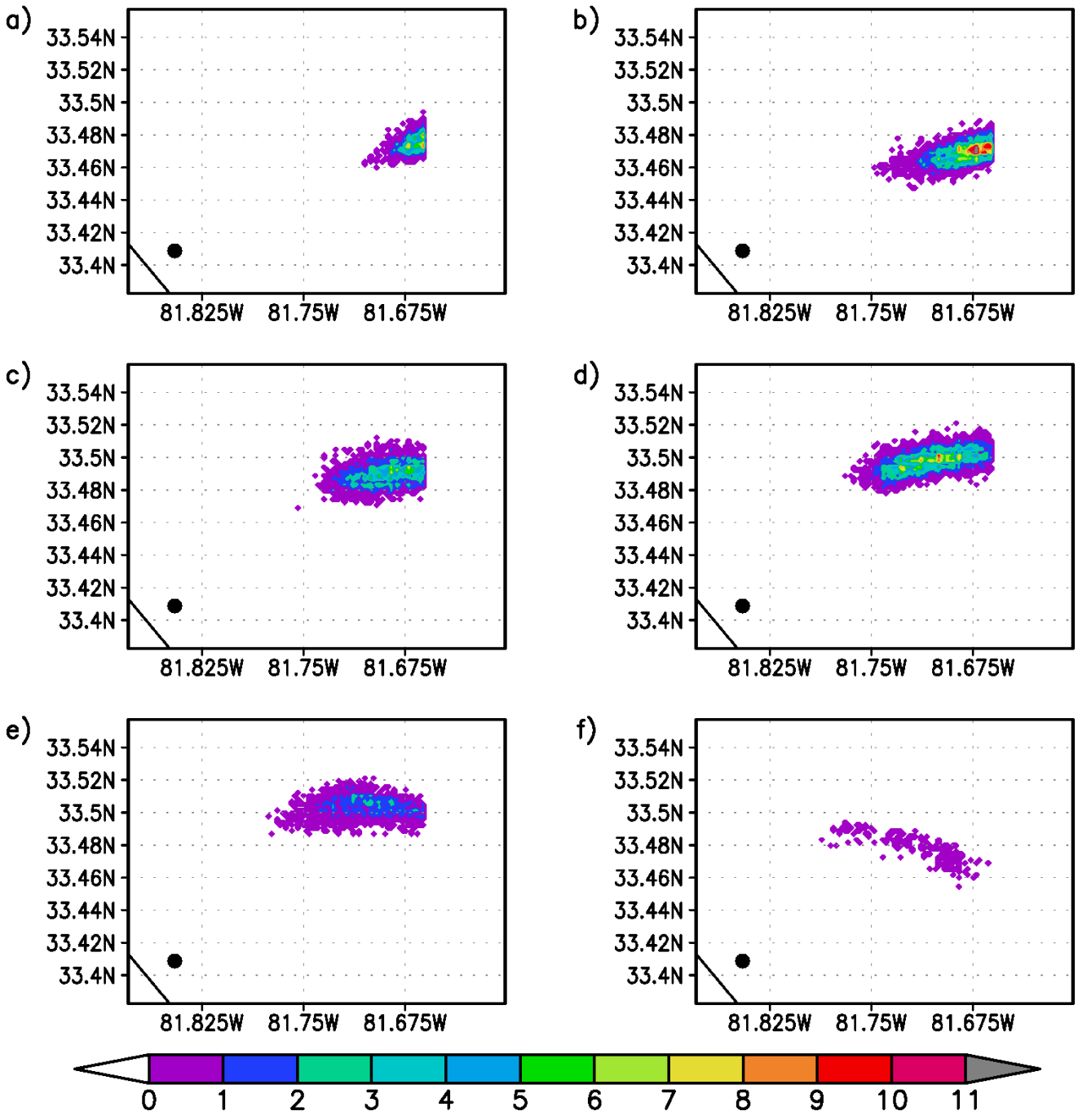
a)
b)
c)
d)
e)
f)
33.54N
33.52N
33.5N
33.48N
33.46N
33.44N
33.42N
33.4N
81.825W
81.75W
81.675W
0
1
2
3
4
5
6
7
8
9
10
11

a)

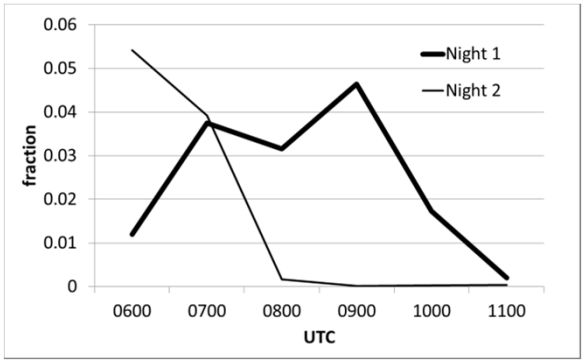
0.06
0.05
0.04
0.03
0.02
0.01
0
fraction
Night 1
Night 2
0600
0700
0800
0900
1000
1100
UTC

b)

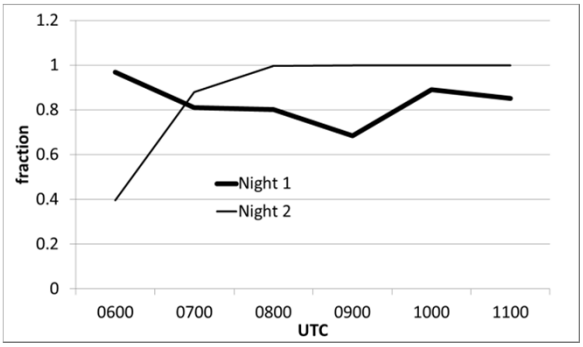
1.2
1
0.8
0.6
0.4
0.2
0
fraction
Night 1
Night 2
0600
0700
0800
0900
1000
1100
UTC

a)

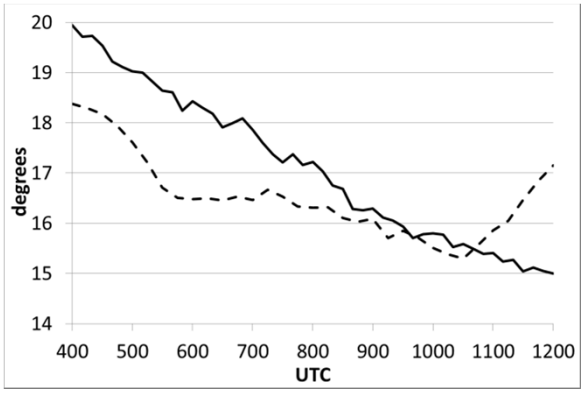
20
19
18
17
16
15
14
degrees
400
500
600
700
800
900
1000
1100
1200
UTC

b)

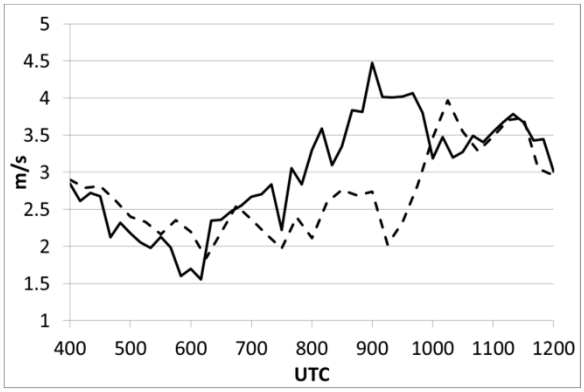
5
4.5
4
3.5
3
2.5
2
1.5
1
m/s
400
500
600
700
800
900
1000
1100
1200
UTC

c)

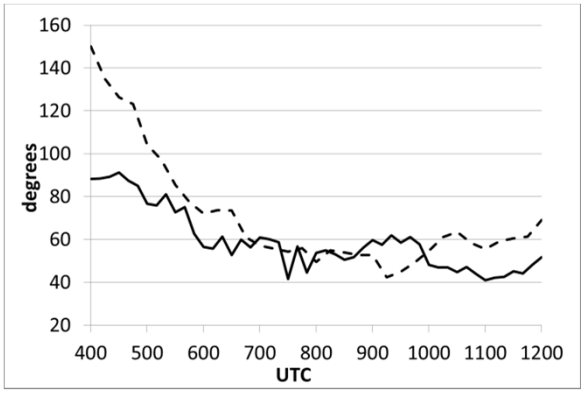
160
140
120
100
80
60
40
20
degrees
400
500
600
700
800
900
1000
1100
1200
UTC

a)

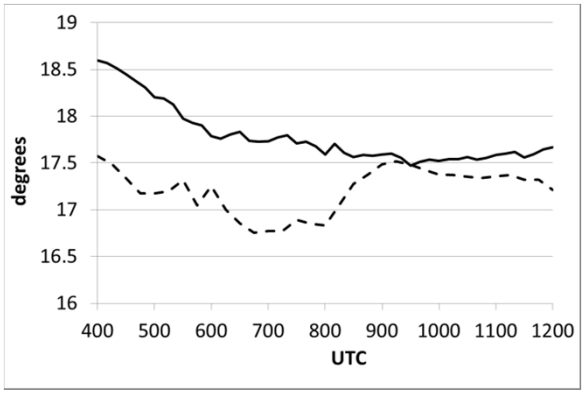
19
18.5
18
17.5
17
16.5
16
degrees
400 500 600 700 800 900 1000 1100 1200
UTC

b)

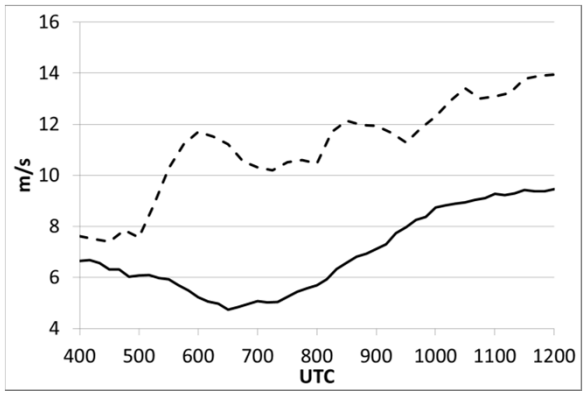
16
14
12
10
8
6
4
m/s
400 500 600 700 800 900 1000 1100 1200
UTC

c)

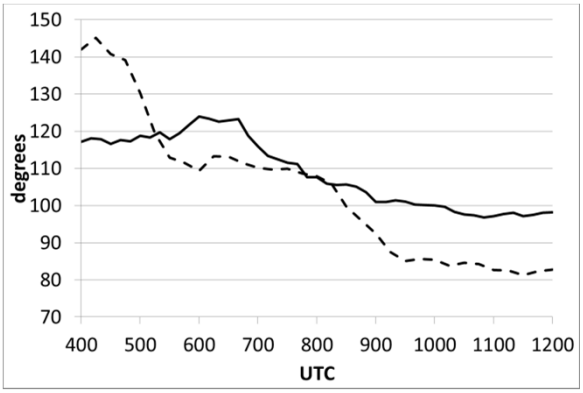
150
140
130
120
110
100
90
80
70
degrees
400 500 600 700 800 900 1000 1100 1200
UTC

a)

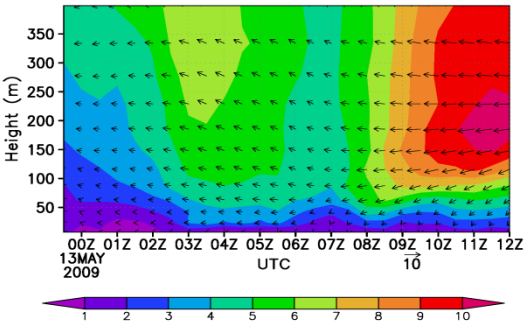
Height (m)
350
300
250
200
150
100
50
00Z 01Z 02Z 03Z 04Z 05Z 06Z 07Z 08Z 09Z 10Z 11Z 12Z
13MAY
2009
UTC
10
1 2 3 4 5 6 7 8 9 10

b)

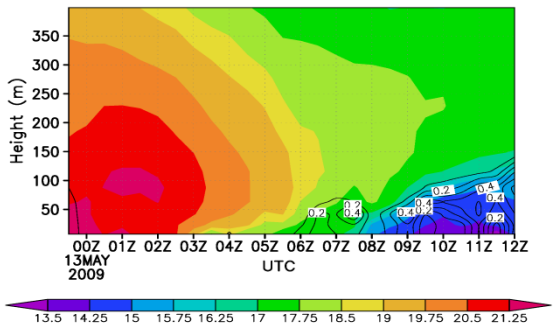
Height (m)
350
300
250
200
150
100
50
00Z 01Z 02Z 03Z 04Z 05Z 06Z 07Z 08Z 09Z 10Z 11Z 12Z
13MAY
2009
UTC
13.5 14.25 15 15.75 16.25 17 17.75 18.5 19 19.75 20.5 21.25

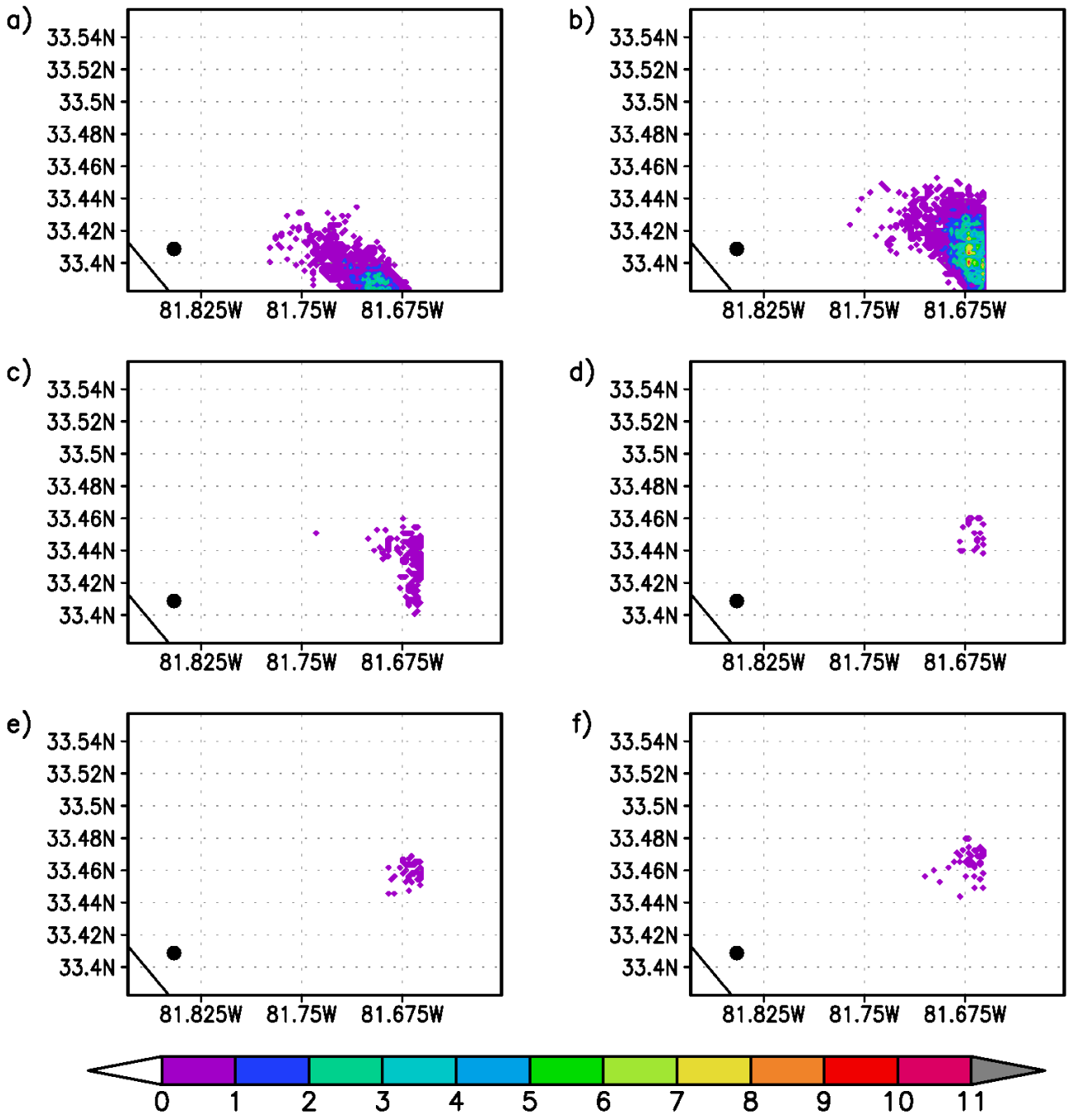
a)
b)
c)
d)
e)
f)
33.54N
33.52N
33.5N
33.48N
33.46N
33.44N
33.42N
33.4N
81.825W
81.75W
81.675W
0
1
2
3
4
5
6
7
8
9
10
11

a)

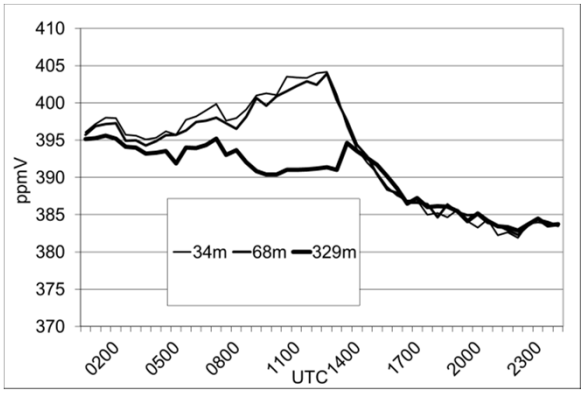
410
405
400
395
390
385
380
375
370
ppmV
34m 68m 329m
0200
0500
0800
1100
1400
1700
2000
2300
UTC

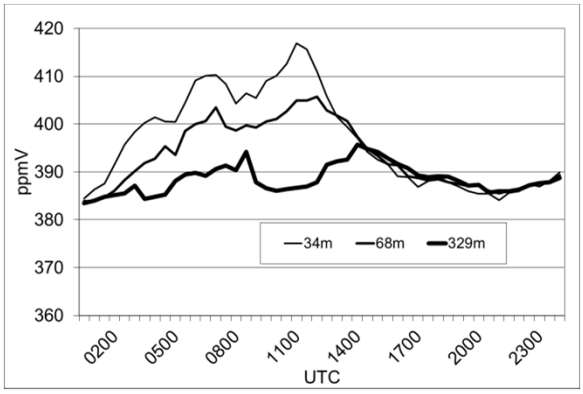
420
410
400
390
380
370
360
ppmV
34m 68m 329m
0200
0500
0800
1100
1400
1700
2000
2300
UTC

b)

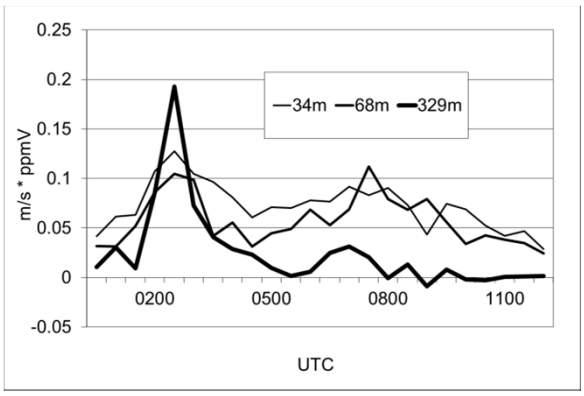
0.25
0.2
0.15
0.1
0.05
0
-0.05
m/s * ppmV
34m 68m 329m
0200
0500
0800
1100
UTC

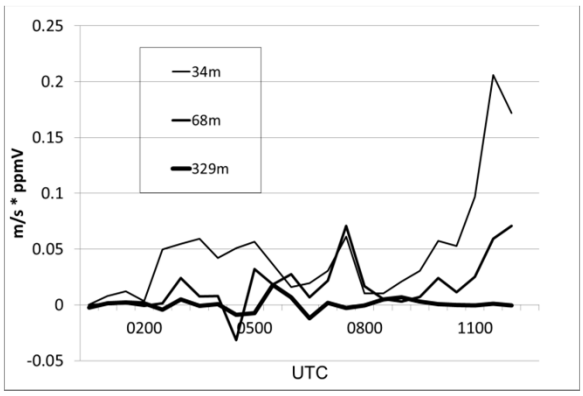
0.25
0.2
0.15
0.1
0.05
0
-0.05
m/s * ppmV
34m
68m
329m
0200
0500
0800
1100
UTC

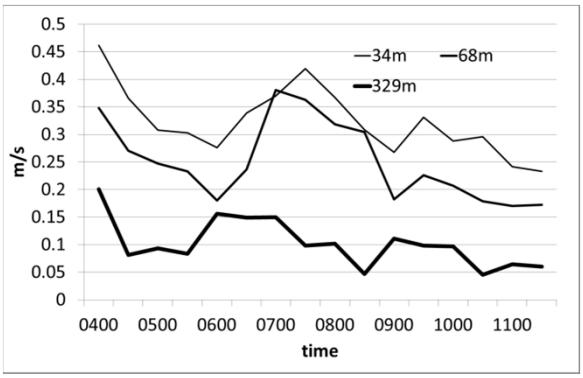
0.5
0.45
0.4
0.35
0.3
0.25
0.2
0.15
0.1
0.05
0
m/s
34m
68m
329m
0400
0500
0600
0700
0800
0900
1000
1100
time

a)

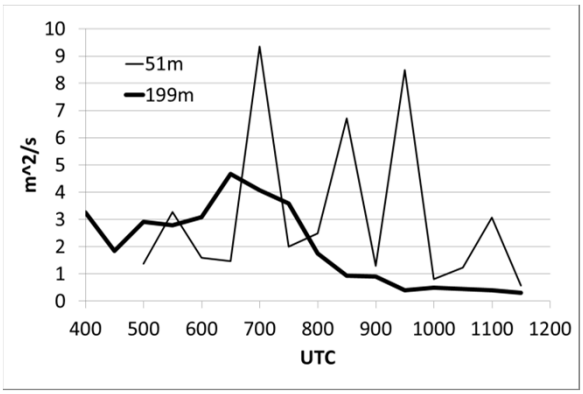
10
9
8
7
6
5
4
3
2
1
0
m^2/s
—51m
199m
400
500
600
700
800
900
1000
1100
1200
UTC

b)

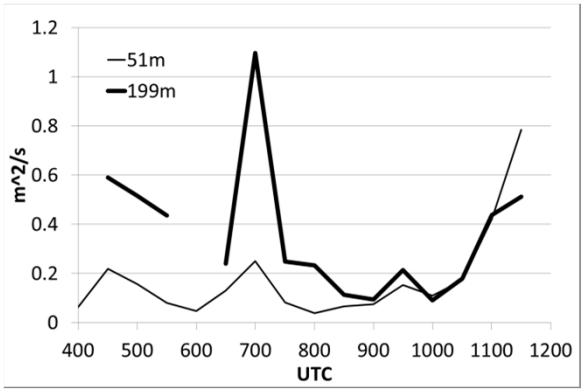
1.2
1
0.8
0.6
0.4
0.2
0
m^2/s
—51m
199m
400
500
600
700
800
900
1000
1100
1200
UTC

Location	Tracer (Night 1)	Tracer (Night 2)
1	O-PDCH	PMCH
2	O-PDCH	PMCP
3	PDCB	PDCB
4	PMCH	PMCH
5	PMCP	PMCP
6	PDCB	PDCB
7	PMCP	PDCB
9	PDCB	PDCH (3x)
10	PMCH	PMCH
11	O-PDCH	PDCH
WA	PTCH	
UE		PTCH

	Night 1		Night 2	
	Rate (g/hr)	Duration (hr)	Rate (g/hr)	Duration (hr)
PDCB	26.5	7.36	27.9	6.99
PMCP	15.5	7.35	16.3	6.99
PMCH	5.0	7.40	7.9	6.96
o-PDCH	2.5	7.60	3.6	6.94
PTCH	1,906	4.00	396	3.25